Supporting Information

Enhancing reverse intersystem crossing through molecular design: insights from strong light–matter coupling in an optical microcavity

Wanlin Cai[a, b], Cheng Zhong[c], Wen-Kai Wu[a], Zhuan-Yun Cai[a], Zi-Wei Ma[a], Yue Qiu[d], Jian-Zhang Zhou[a], and De-Yin Wu*[a]

[a] *State Key Laboratory of Physical Chemistry of Solid Surface, Collaborative Innovation Center of Chemistry for Energy Materials, and Department of Chemistry, College of Chemistry and Chemical Engineering, Xiamen University, Xiamen, 361005, P. R. China*

[b] *Fujian Key Laboratory of Flexible Electronics, Strait Institute of Flexible Electronics (SIFE Future Technologies), Fujian Normal University, Fuzhou, Fujian 350117, P. R. China.*

[c] *Hubei Key Lab on Organic and Polymeric Optoelectronic Materials, Department of Chemistry, Wuhan University, Wuhan, Hubei 430072, P. R. China*

[d] *Grimwade Centre for Cultural Materials Conservation, School of Historical and Philosophical Studies, Faculty of Arts University of Melbourne, Parkville, VIC 3052, Australia*

E-mail: dywu@xmu.edu.cn

Table of Contents

Reason for the large $\Delta E^{0-0}_{S_1(S_0)-T_1}$ of the β-fused thiophene derivatives

The β-fused thiophene derivatives (S1_1, S2_1, S3_1, and S4_1) exhibit a high $\Delta E^{0-0}_{S_1(S_0)-T_1}$ above 0.8 eV, which is mainly attributed to their low triplet excited energy (**Figure S2**). This low triplet excited energy can be interpreted as a result of the weak antiaromaticity in T_1, contributing to the stabilization of the triplet state energy of the β-fused derivatives.[1,2] As shown in **Figure S3**, the values of the nucleus-independent chemical shifts placed above the ring in T_1 (NICIS(1) ZZ,T_1) of ring_2/ring_2' and ring_5 in the β-fused derivatives are much lower than those in the α-fused thiophene derivatives (S1_2, S1_3, S2_2, S2_3, S3_2, S3_3, S4_2, and, S4_3).[3] This difference reveals that the antiaromaticity in T_1 of the β-fused derivatives is weaker than that of the α-fused thiophene derivatives. Here, a higher positive NICIS(1) ZZ,T_1 value indicates stronger antiaromaticity, while a more negative value indicates stronger aromaticity.

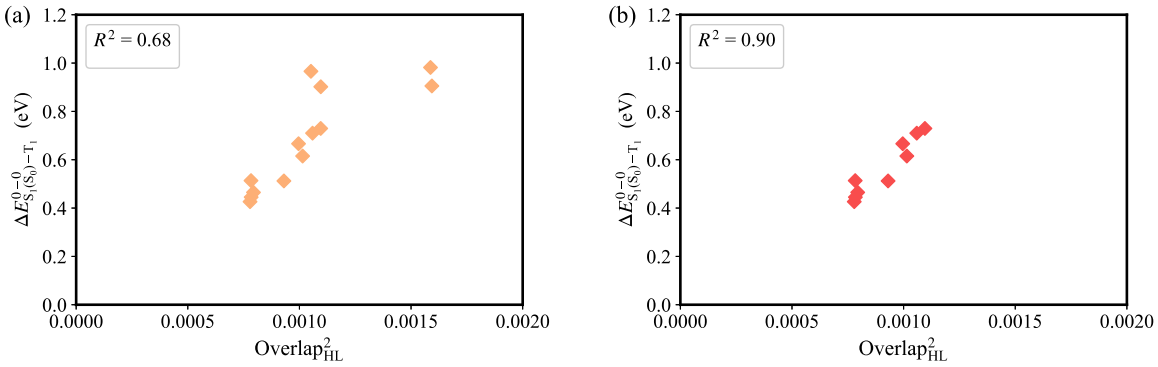

Figure S1. Linear regression fits of Overlap^2_{HL} and $\Delta E^{0-0}_{S_1(S_0)-T_1}$ for (a) all studied molecules and (b) BisICz and α-fused thiophene derivatives.

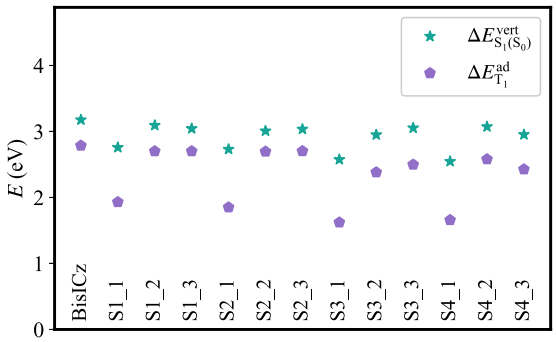

Figure S2. Calculated vertical S_1 excitation energy based on the ground geometry and adiabatic T_1 excitation energy.

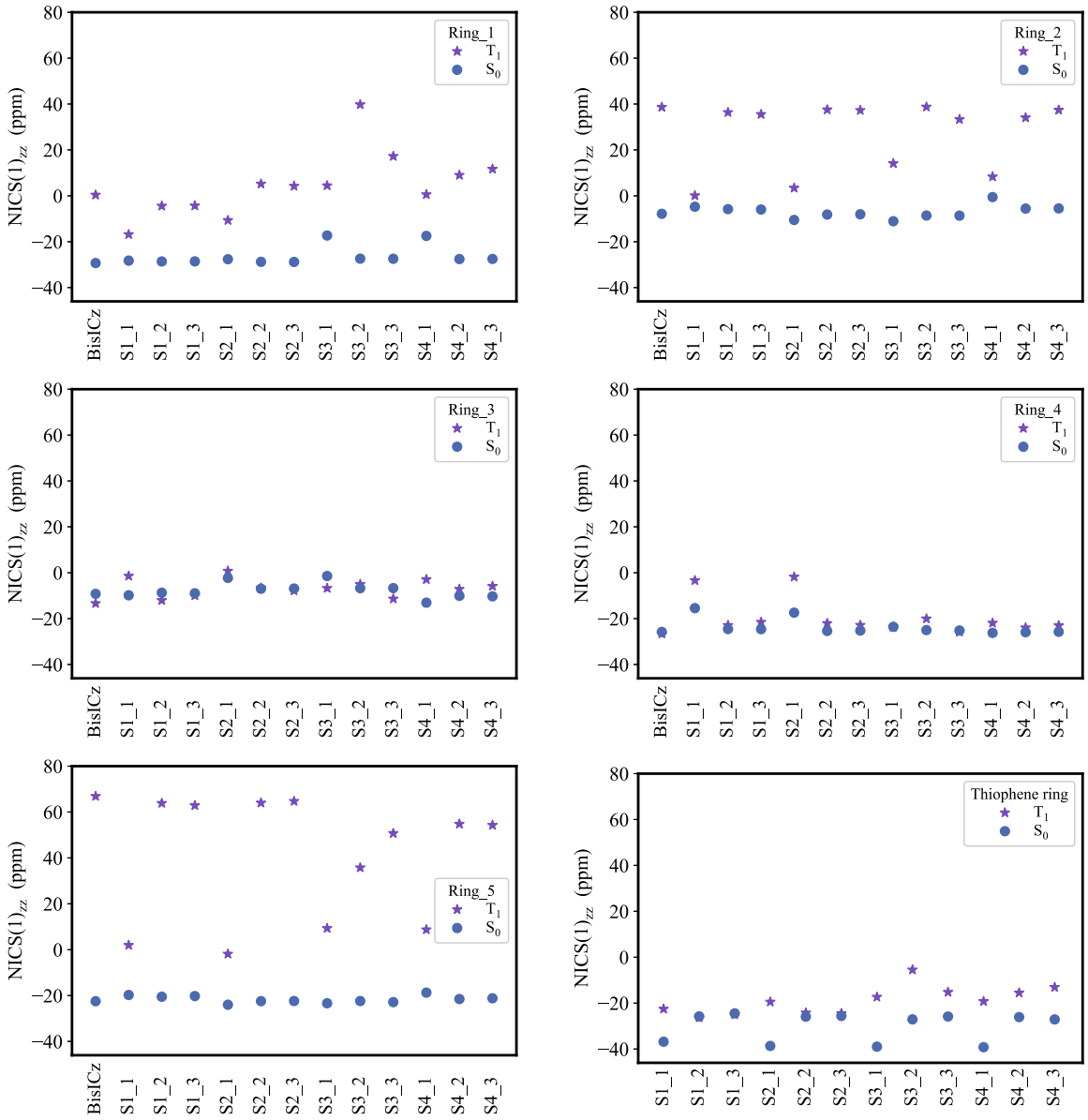

Figure S3. The nucleus-independent chemical shifts placed above the ring ($NICS(1)_{zz}$) in S_0 and T_1.

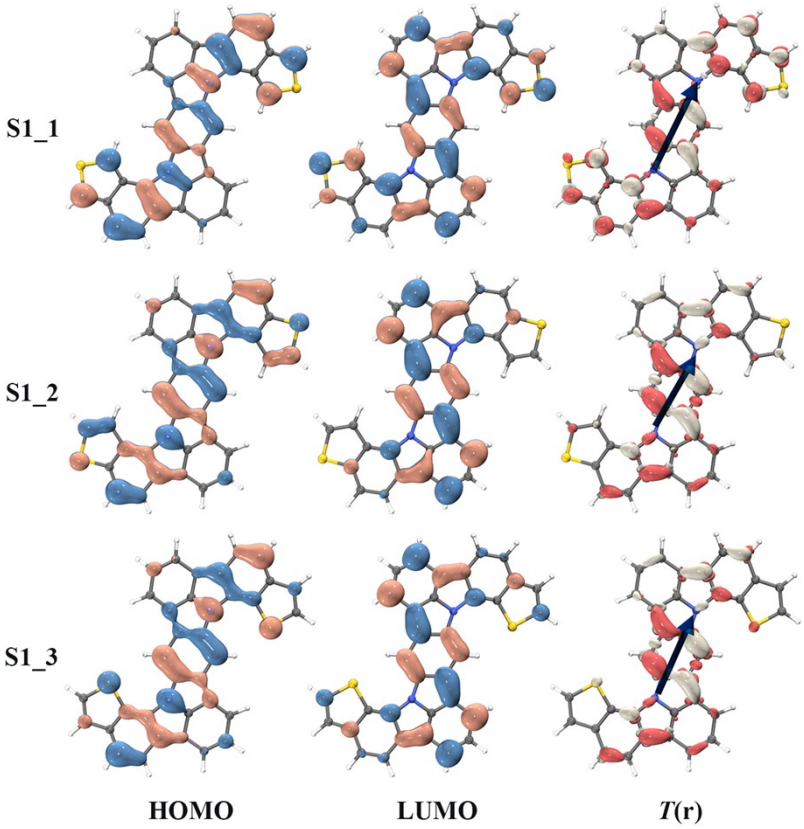

Figure S4. The HOMO and LUMO distribution (isovalue = 0.03 au) and transition density $T(r)$ of S_1 excitation (isovalue = 0.0012 au), for S1_1, S1_2, and S1_3.

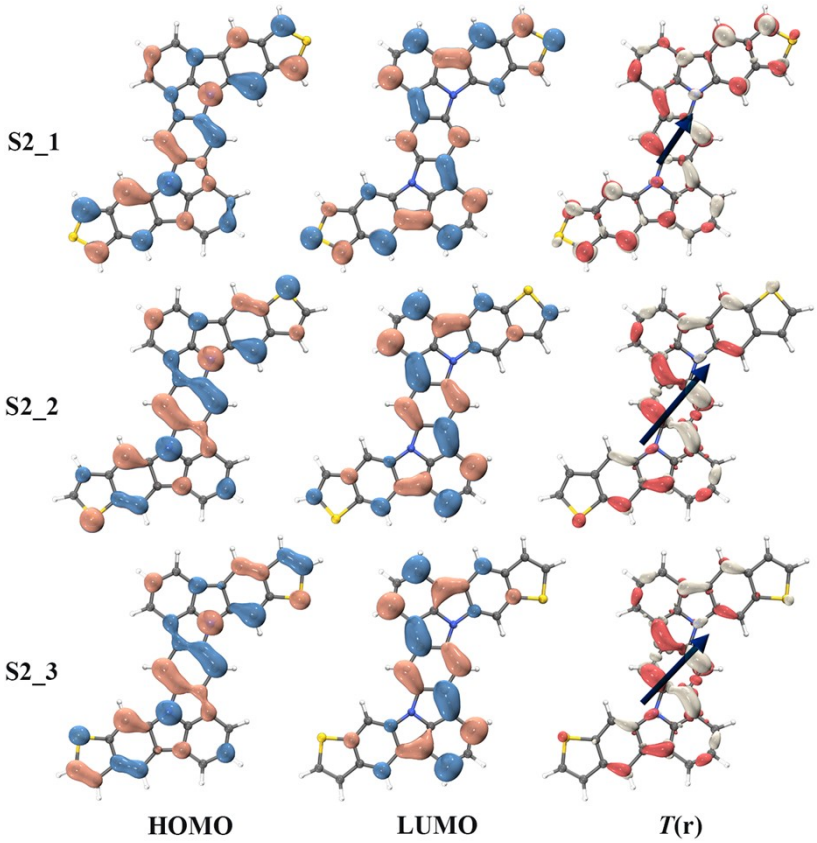

Figure S5. The HOMO and LUMO distribution (isovalue = 0.03 au) and transition density $T(r)$ of S_1 excitation (isovalue = 0.0012 au), for S2_1, S2_2, and S2_3.

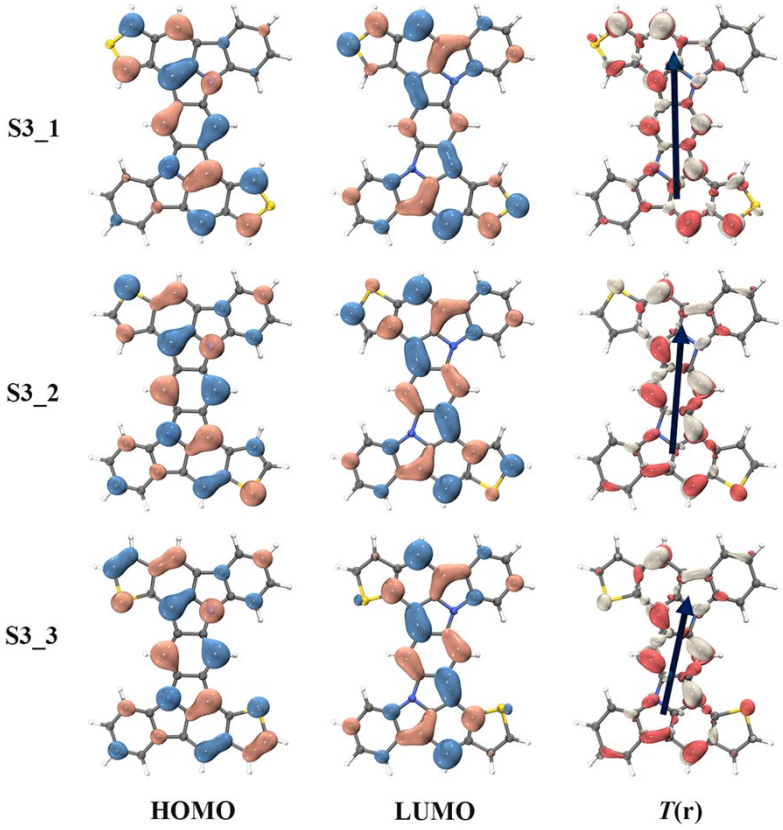

Figure S6. The HOMO and LUMO distribution (isovalue = 0.03 au) and transition density $T(r)$ of S_1 excitation (isovalue = 0.0012 au), for S3_1, S3_2, and S3_3.

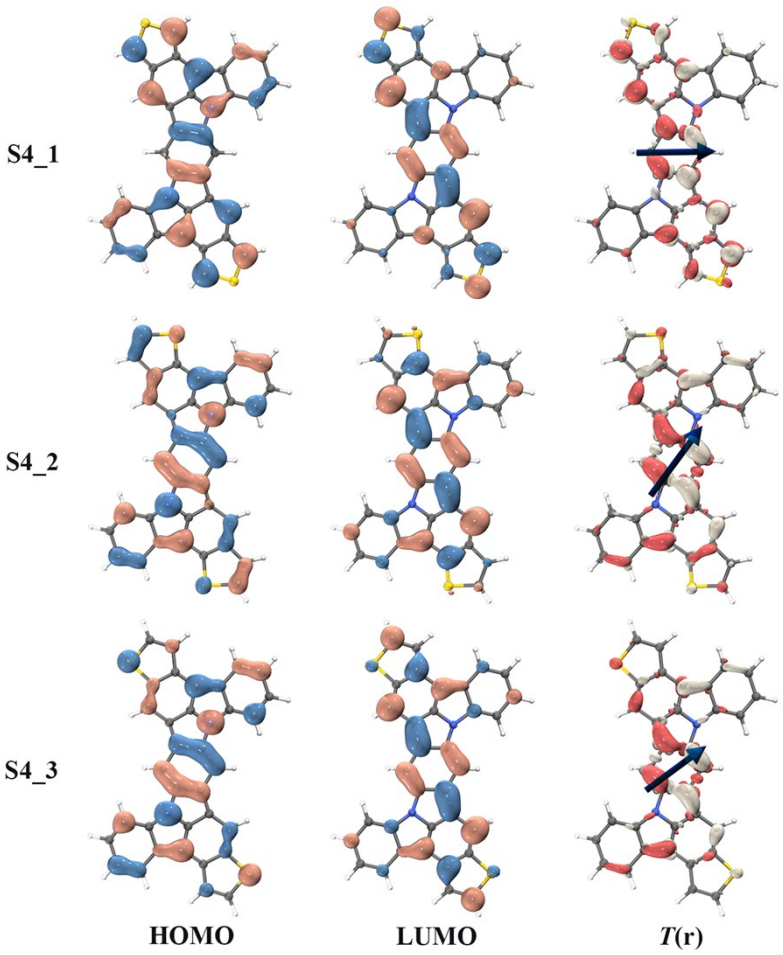

Figure S7. The HOMO and LUMO distribution (isovalue = 0.03 au) and transition density $T(r)$ of S_1 excitation (isovalue = 0.0012 au), for S4_1, S4_2, and S4_3.

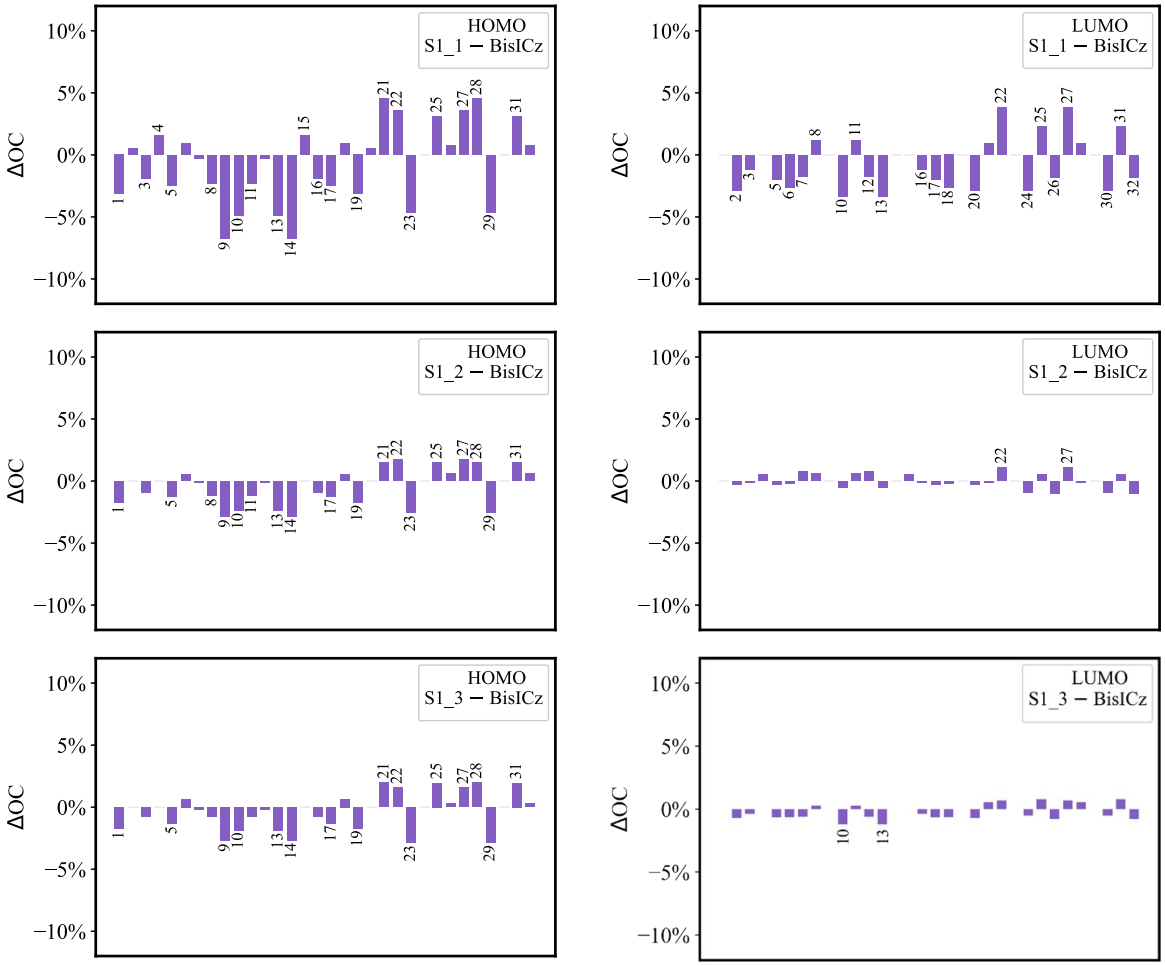

Figure S8. The variation of orbital composition ($\Delta OC_{S1\_1/S1\_2/S1\_3 - BisICz}$) on atoms.

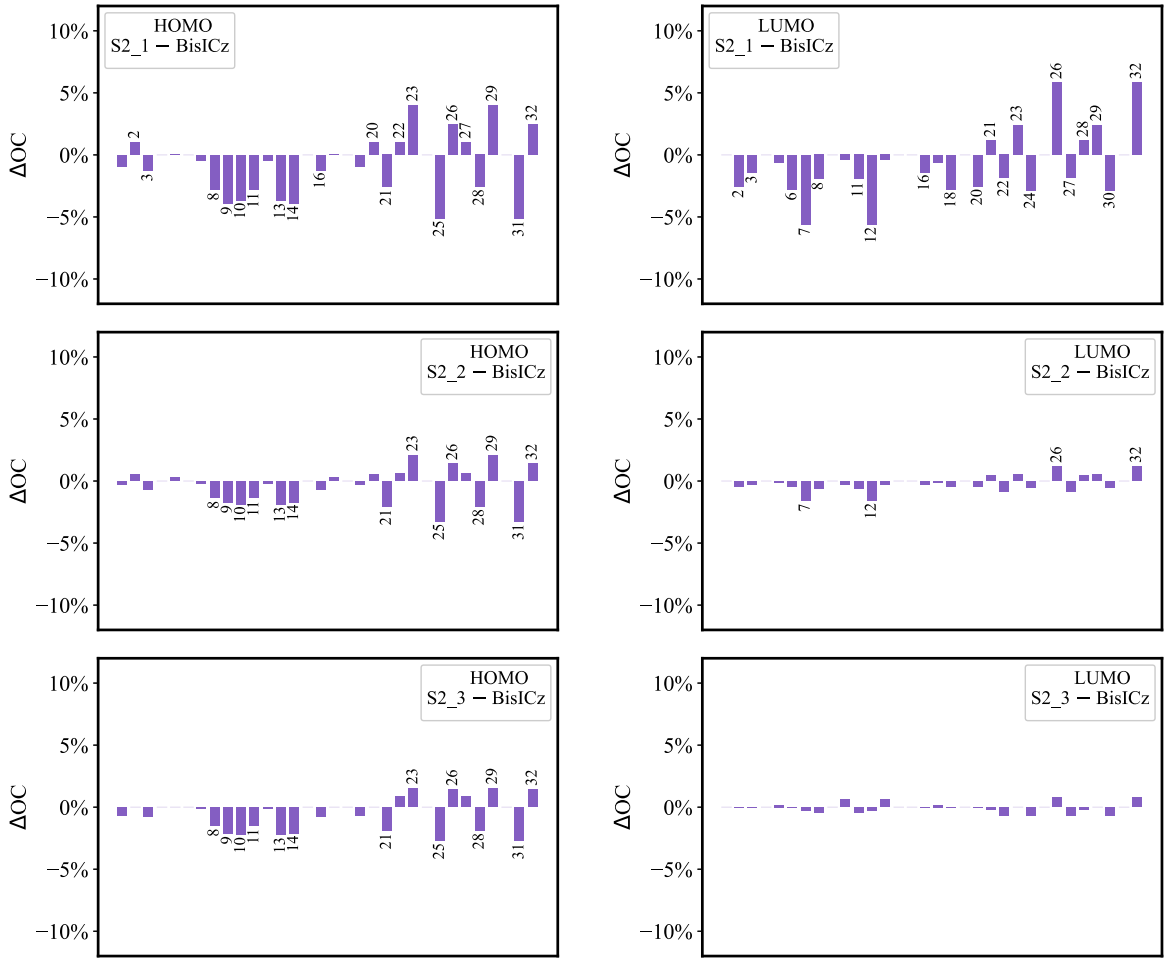

Figure S9. The variation of orbital composition ($\Delta OC_{S2\_1/S2\_2/S2\_3 - BisICz}$) on atoms.

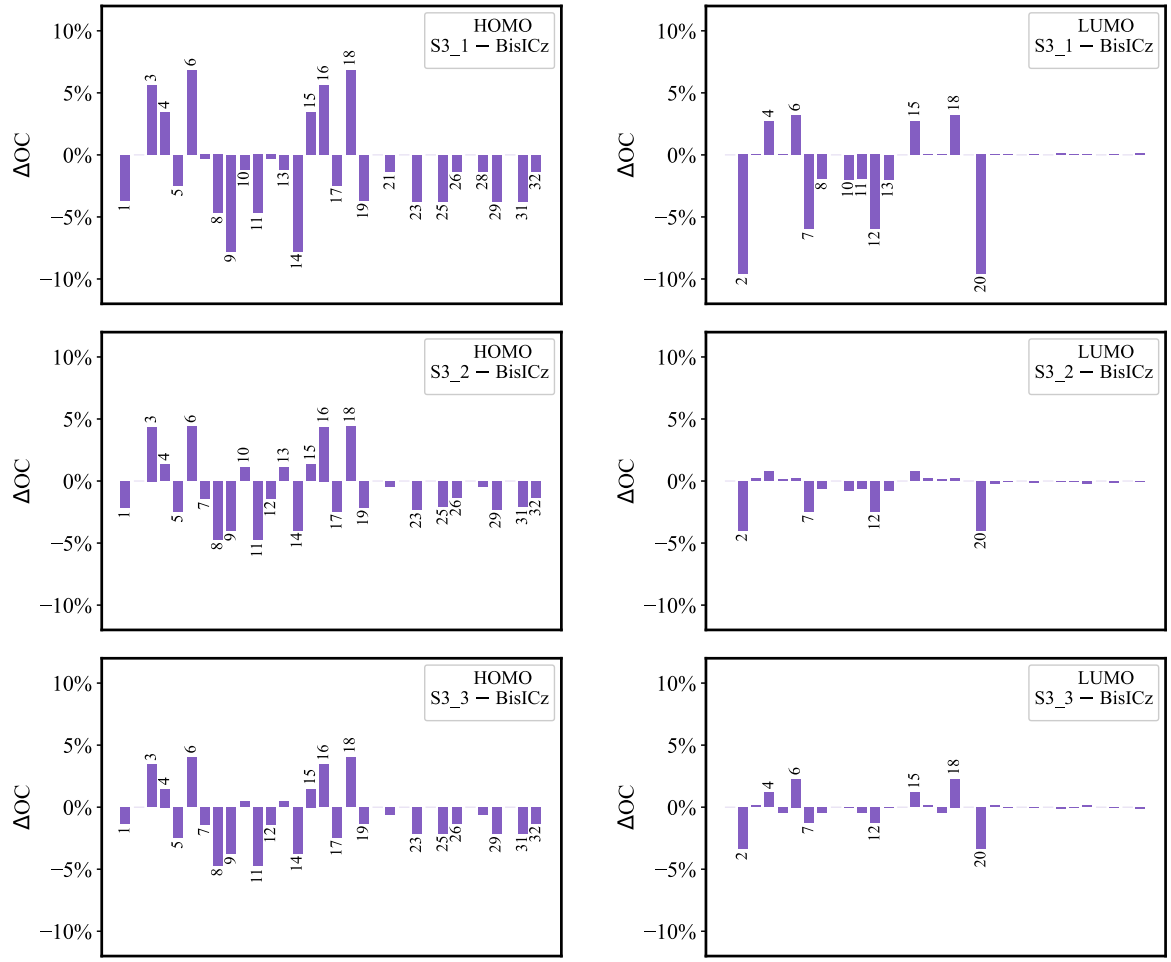

Figure S10. The variation of orbital composition ($\Delta OC_{S3\_1/S3\_2/S3\_3 - BisICz}$) on atoms.

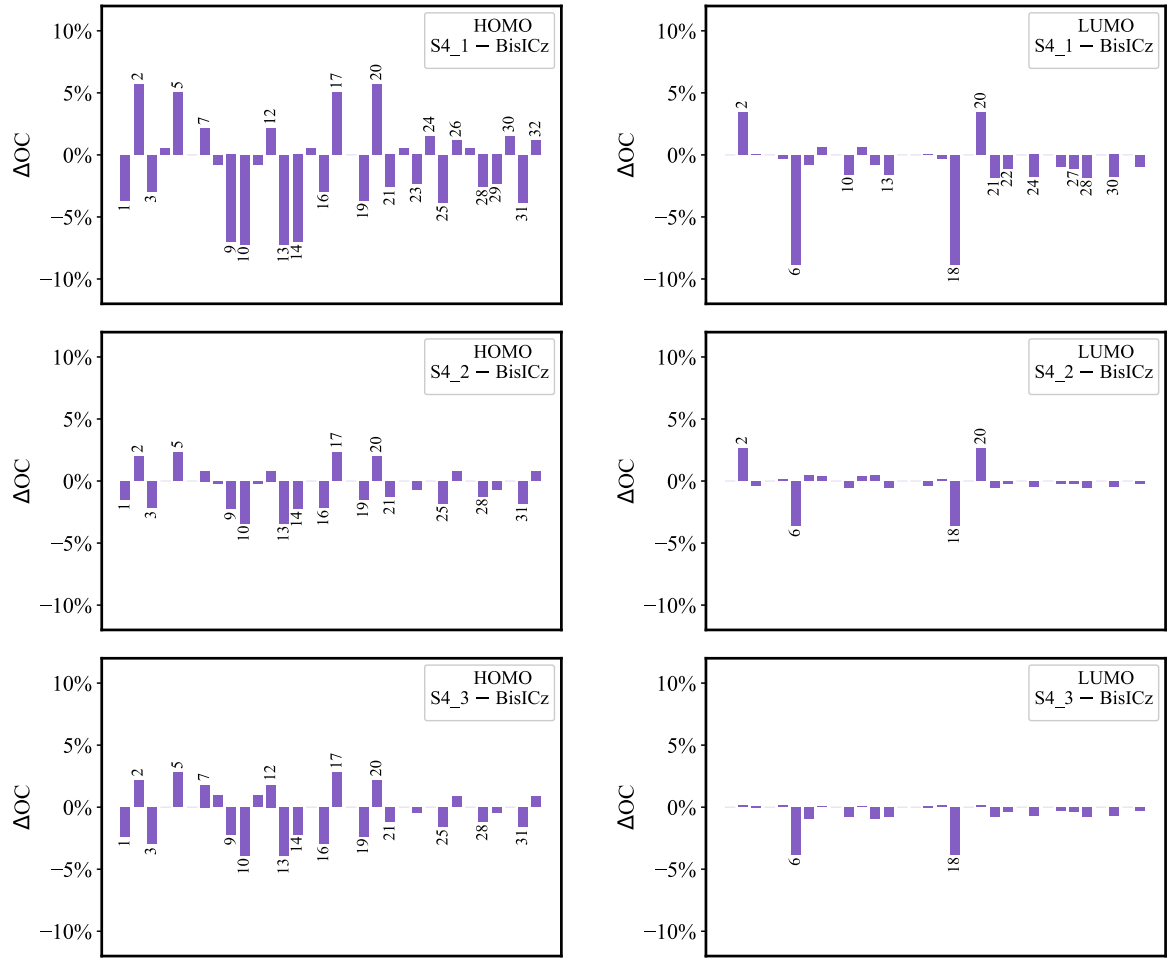

Figure S11. The variation of orbital composition ($\Delta OC_{S4\_1/S4\_2/S4\_3 - BisICz}$) on atoms.

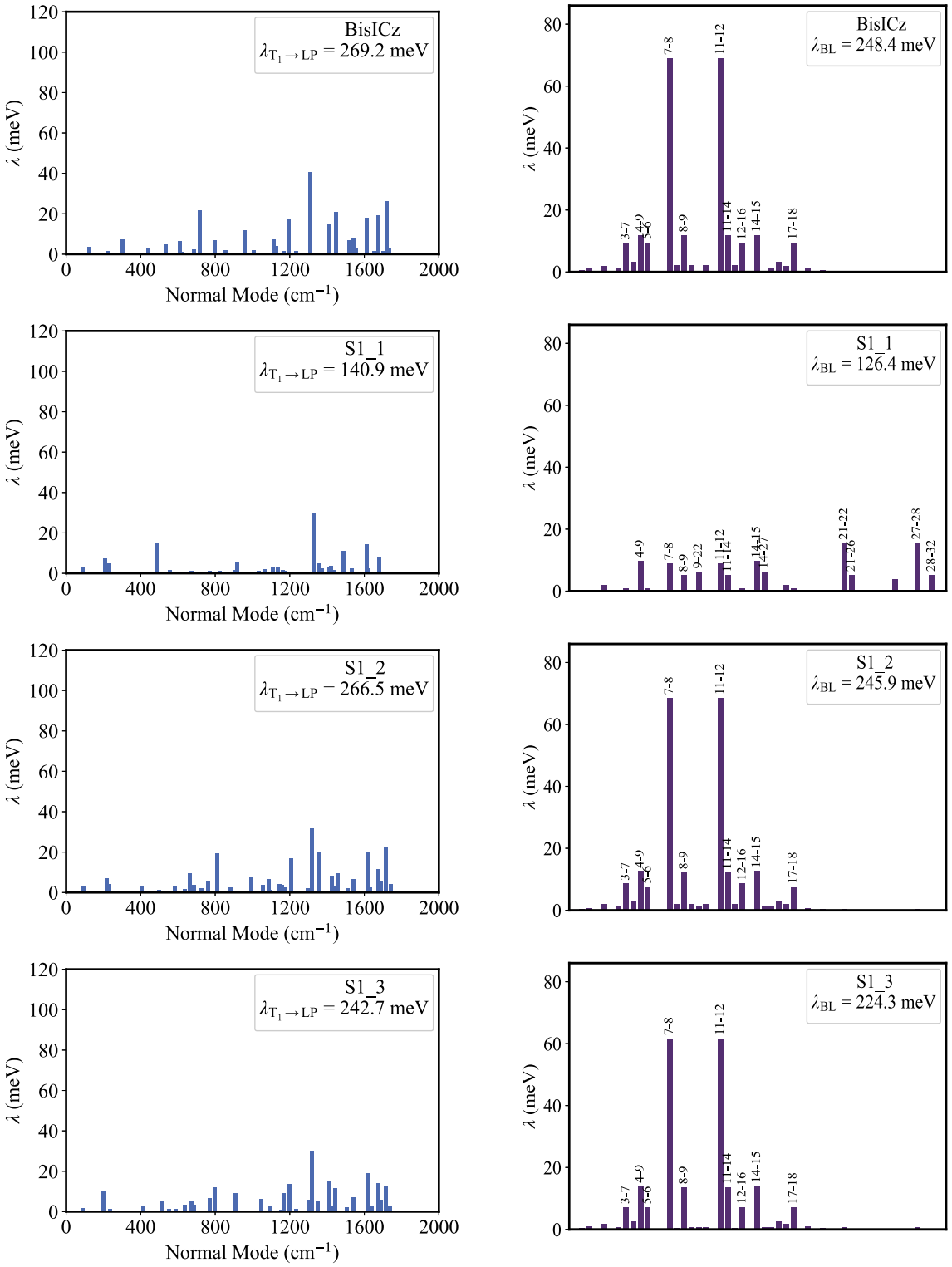

Figure S12. The contribution of the normal modes to the reorganization energy (left), and the contribution of chemical bonds to the reorganization energy (right), for BisICz, S1_1, S1_2, and S1_3.

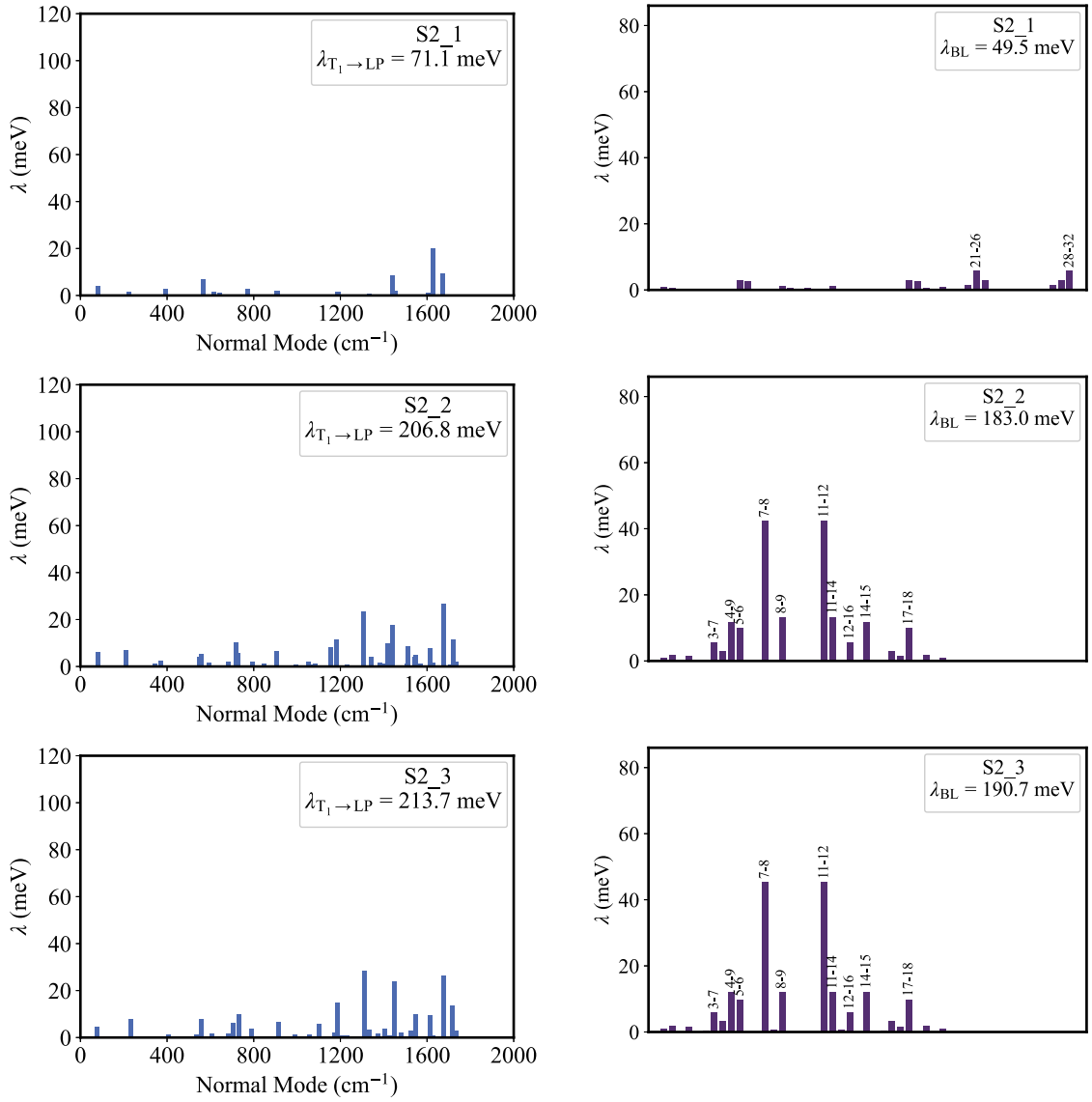

Figure S13. The contribution of the normal modes to the reorganization energy (left), and the contribution of chemical bonds to the reorganization energy (right), for S2_1, S2_2, and S2_3.

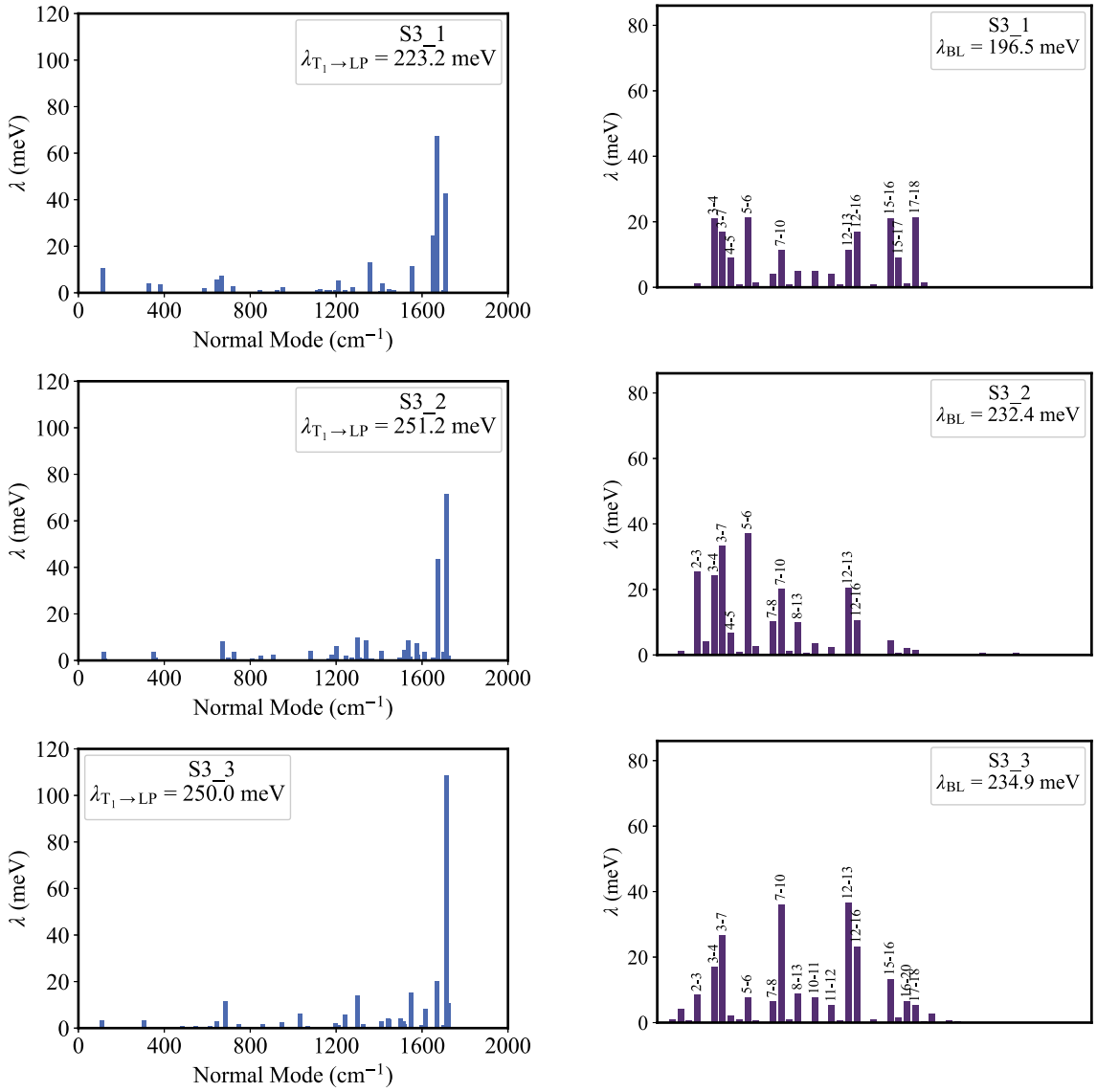

Figure S14. The contribution of the normal modes to the reorganization energy (left), and the contribution of chemical bonds to the reorganization energy (right), for S3_1, S3_2, and S3_3.

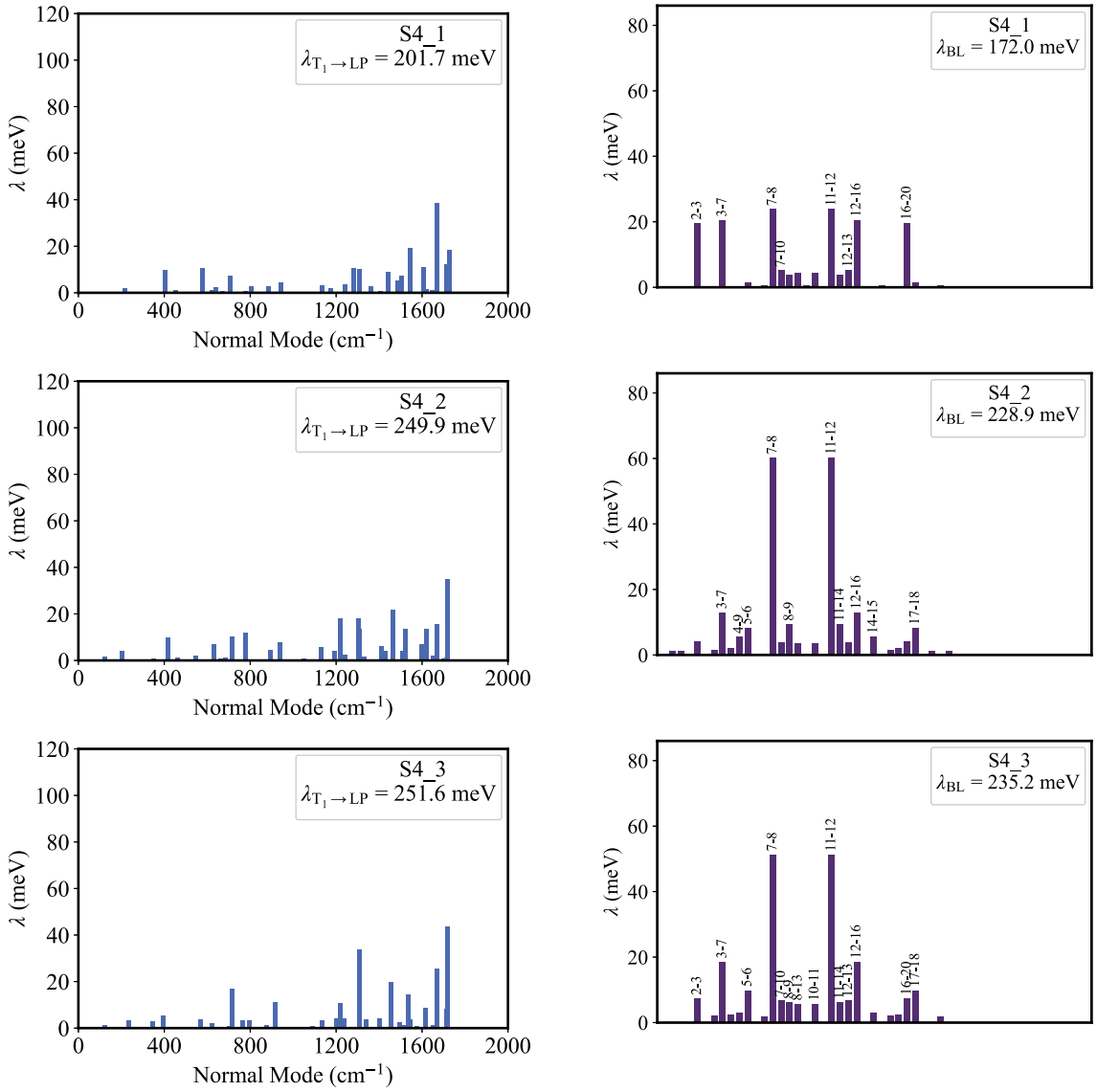

Figure S15. The contribution of the normal modes to the reorganization energy (left), and the contribution of chemical bonds to the reorganization energy (right), for S4_1, S4_2, and S4_3.

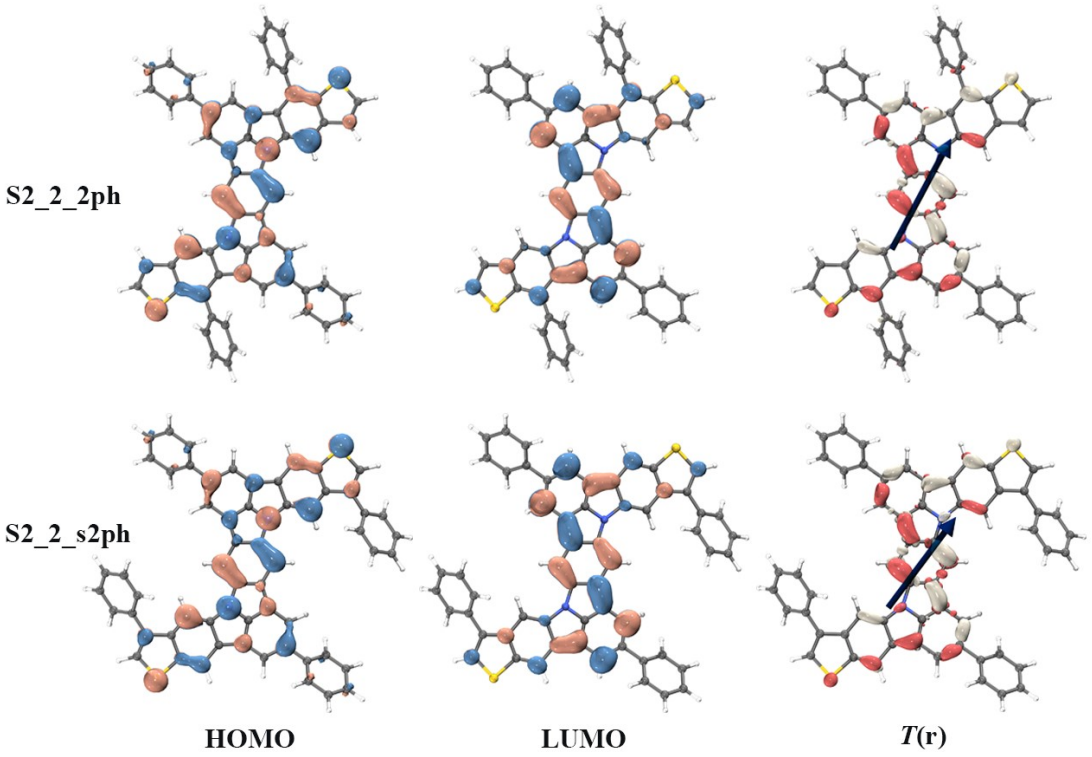

Figure S16. HOMO and LUMO distribution (isovalue = 0.03 au) and transition density $T(\mathrm{r})$ of S_1 excitation (isovalue = 0.0012 au), for S2_2_2ph and S2_2_s2ph.

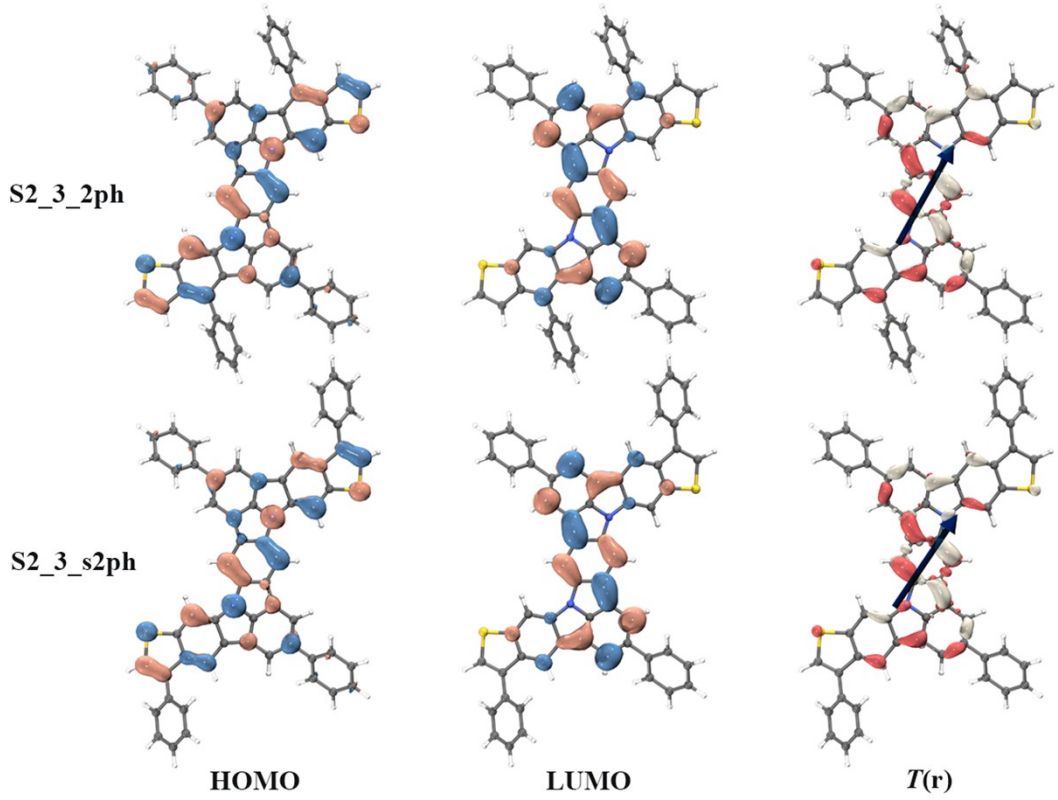

Figure S17. HOMO and LUMO distribution (isovalue = 0.03 au) and transition density $T(r)$ of S_1 excitation (isovalue = 0.0012 au), for S2_3_2ph and S2_3_s2ph.

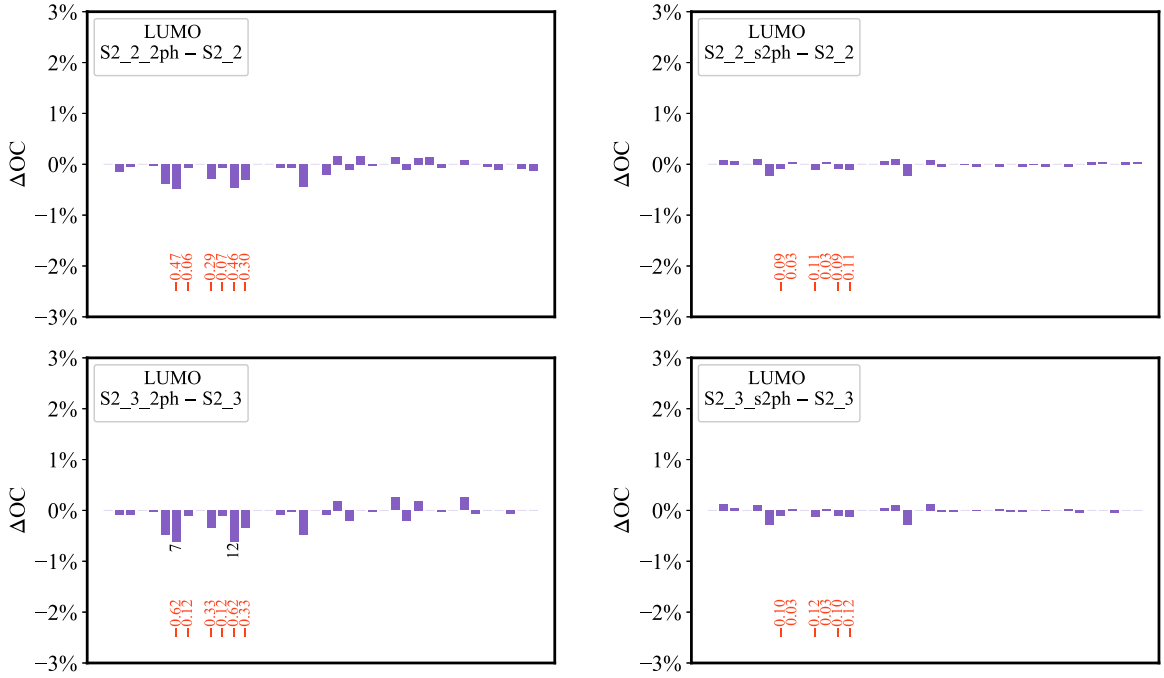

Figure S18. The variation of LUMO orbital composition ($\Delta OC_{S2\_2\_2ph/S2\_2\_s2ph\ -\ S2\_2}$, $\Delta OC_{S2\_3\_2ph/S2\_3\_s2ph\ -\ S2\_3}$) on atoms.

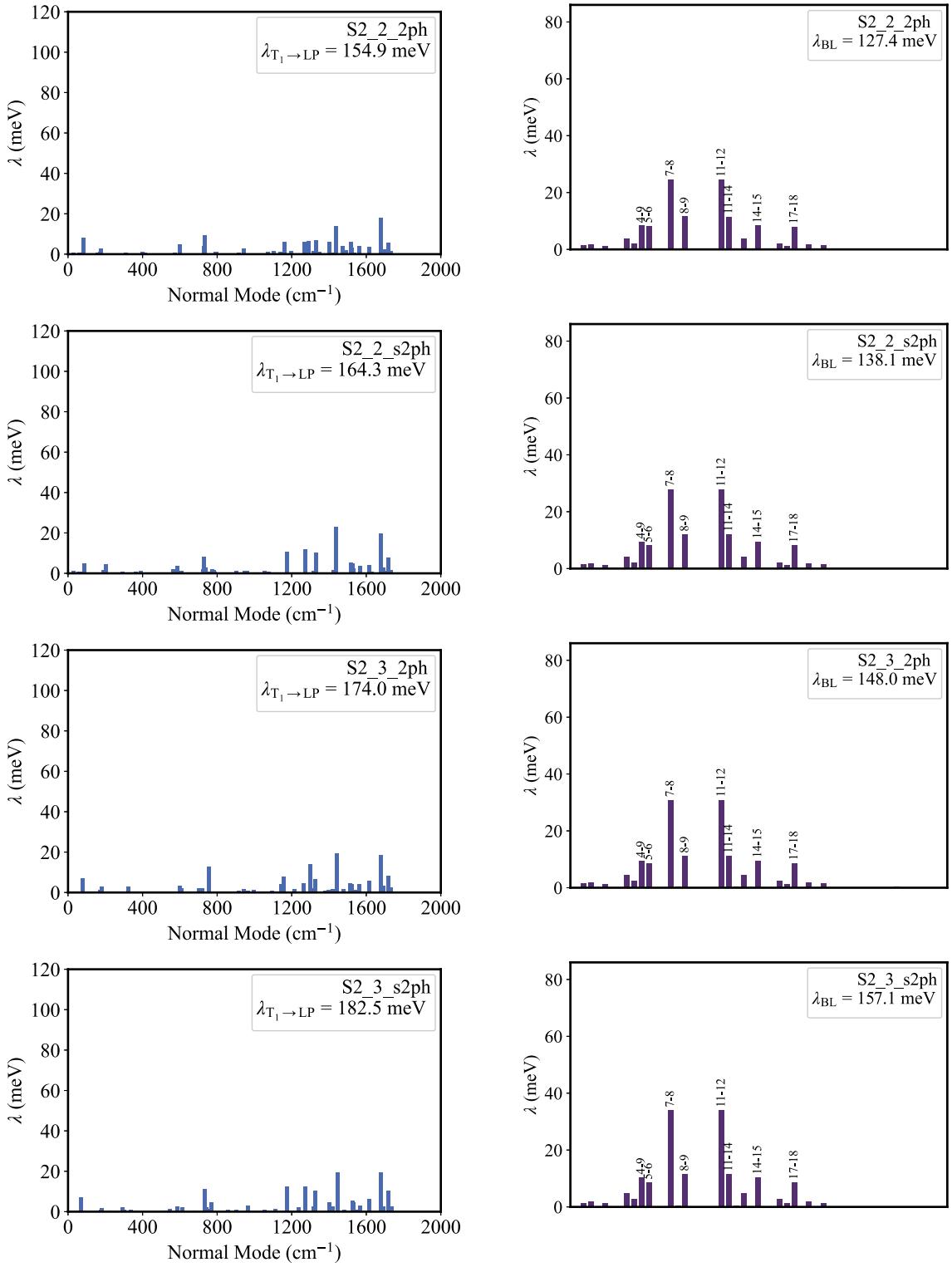

Figure S19. The contribution of the normal modes to the reorganization energy (left), and the contribution of chemical bonds to the reorganization energy (right), for S2_2_2ph, S2_2_s2ph, S2_3_2ph, and S2_3_s2ph.

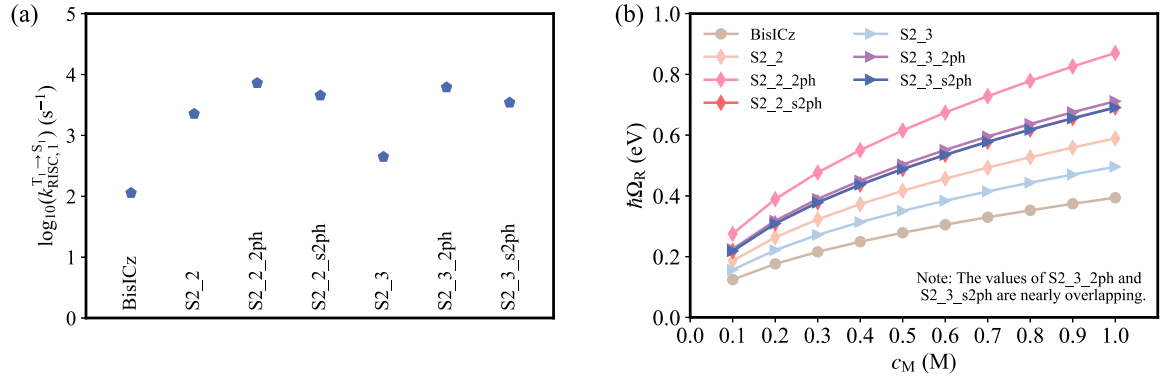

Figure S20. Calculated (a) $k_{RISC}^{T_1\rightarrow S_1}$ outside the cavity, (b) $\hbar\Omega_R$ inside the cavity, for BisICz and S2_2, S2_2_2ph, S2_2_s2ph, S2_3, S2_3_2ph, and S2_3_s2ph.

References

1. K. J. Fallon, P. Budden, E. Salvadori, A. M. Ganose, C. N. Savory, L. Eyre, S. Dowland, Q. Ai, S. Goodlett and C. Risko, Exploiting excited-state aromaticity to design highly stable singlet fission materials, *J. Am. Chem. Soc.*, 2019, **141**, 13867-13876.
2. O. El Bakouri, J. R. Smith and H. Ottosson, Strategies for design of potential singlet fission chromophores utilizing a combination of ground-state and excited-state aromaticity rules, *J. Am. Chem. Soc.*, 2020, **142**, 5602-5617.
3. T. Lu and F. Chen, Multiwfn: a multifunctional wavefunction analyzer, *J. Comput. Chem.*, 2012, **33**, 580-592.